ISSN 2072-5981
doi: 10.26907/mrsej

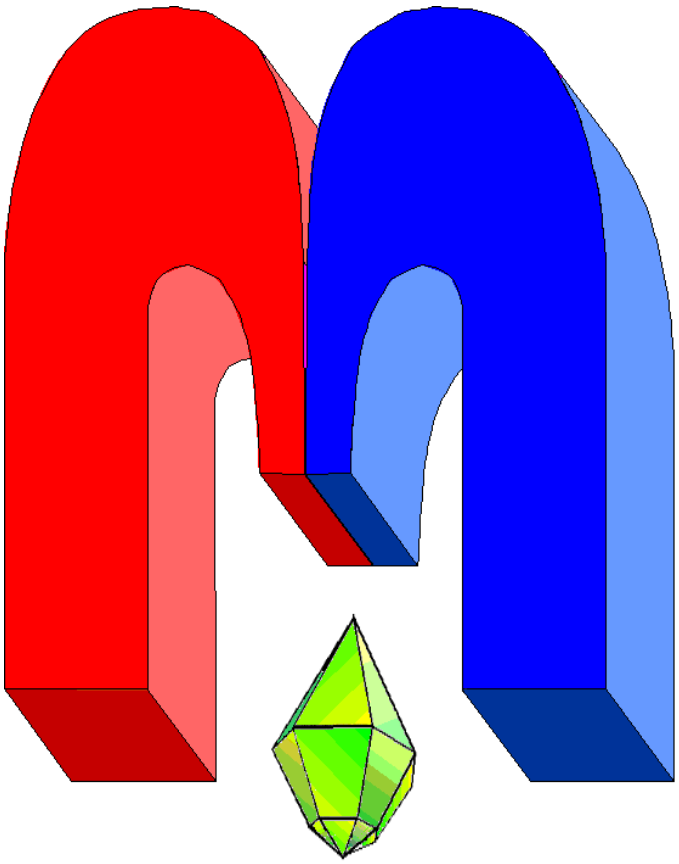

Magnetic Resonance in Solids

Electronic Journal

Volume 27
Issue 3
Article No ***25306***
1-10 pages
2025
doi: **10.26907/mrsej-25306**

http://mrsej.kpfu.ru
http://mrsej.elpub.ru

Established and published by Kazan University*
Endorsed by International Society of Magnetic Resonance (ISMAR)
Registered by Russian Federation Committee on Press (#015140), August 2, 1996
First Issue appeared on July 25, 1997

"***Magnetic Resonance in Solids. Electronic Journal***" (**MRS*ej***) is a peer-reviewed, all electronic journal, publishing articles which meet the highest standards of scientific quality in the field of basic research of a magnetic resonance in solids and related phenomena.

Indexed and abstracted by
Web of Science (ESCI, Clarivate Analytics, from 2015),White List (from 2023) *Scopus* (Elsevier, from 2012), *RusIndexSC* (*eLibrary*, from 2006), *Google Scholar*, *DOAJ*, *ROAD*, *CyberLeninka* (from 2006), *SCImago Journal & Country Rank*, etc.

* Address: "Magnetic Resonance in Solids. Electronic Journal", Kazan Federal University; Kremlevskaya str., 18; Kazan 420008, Russia

† In Kazan University the Electron Paramagnetic Resonance (EPR) was discovered by Zavoisky E.K. in 1944.

Nuclear quadrupole interaction of a negatively charged boron vacancy with near and far nitrogen nuclei in hexagonal boron nitride: a combined density functional and electron paramagnetic resonance study

E.V. Dmitrieva[1,*], D.V. Shurtakova[1], G.V. Mamin[1], I.N. Gracheva[1], F.F. Murzakhanov[1], S.S. Nagalyuk[2], V.A. Soltamov[2], M.R. Gafurov[1]

[1]Kazan Federal University, Kazan 420008, Russia

[2]Ioffe Institute, St.Petersburg 194021, Russia

**E-mail: dev600@mail.ru*

(received October 20, 2025; revised December 3, 2025; accepted December 6, 2025; published December 13, 2025)

The negatively charged boron vacancy in hexagonal boron nitride is one of the most prominent representatives of an optically active qubit in two-dimensional van der Waals materials. In this case, the electron-nuclear interactions of the vacancy with the magnetic moments of the hBN lattice atoms are of particular interest. In this paper, we investigated the nuclear quadrupole interactions of the boron vacancy with the removed nuclear spins of nitrogen ^{14}N ($I = 1$) using the method of electron-nuclear double resonance. The constant of the corresponding quadrupole interaction is determined and the type of the corresponding tensor is determined. A comparative analysis of the obtained parameters of the nuclear quadrupole interaction with the parameters for the nitrogen atoms closest to the vacancy is carried out. Based on the data presented, it is proposed to use the electron spin of the boron vacancy as a spin probe to study the fundamental properties of boron nitride, such as the constants of the nuclear quadrupole interaction.

PACS: 71.70.-d, 71.70.Jp, 75.10.Dg, 76.30.-v, 76.70.Dx, 76.30.Mi, 73.90.+f

Keywords: ESR, ENDOR, boron vacancy, hBN, nuclear quadrupole interaction

1. Introduction

Hexagonal boron nitride (hBN) a two-dimensional van der Waals material with a wide band gap (~6 eV) [1, 2], has become one of the key objects in the field of quantum technologies [2–6] and two-dimensional nanoelectronics based on van der Waals heterostructures [2, 3, 7] in recent years. In particular, point defects in hBN are used to create single photon sources for quantum telecommunications [2, 3, 5, 8], quantum sensors for magnetic fields, temperature, and pressure [9, 10], as well as new approaches to optical polarization of nuclear spins [11, 12]. Of particular interest in this context are optically active point defects in hBN, which have the property of polarization of electron spin states under the action of optical pumping, which were first discovered in hBN in [6, 8]. Thus, in [6], an unambiguous identification of such a defect was carried out in the form of a negatively charged boron vacancy ($V_{\mathbf{B}}^{-}$) structure, the spin and optical properties of which are shown in Fig. 1(a). The $V_{\mathbf{B}}^{-}$ defect has a basic triplet ($S = 1$) state optically induced by the inverse occupancy of the spin sublevel $m_S = 0$ at room temperature and, due to the spin-dependent optical recombination channel from the excited (ES) to the ground state (GS) through the metastable level (MS), the ability to register an optically detected magnetic resonance (ODMR) signal. No such unambiguous identification was carried out in [8], however, it was suggested that point defects associated with carbon impurity may have optical polarization of electron spins at room temperature, which allowed the authors of the article to demonstrate the reading of the electron spins of these defects by ODMR. The results of these two studies gave pulse to the rapid development of studies of optically addressable

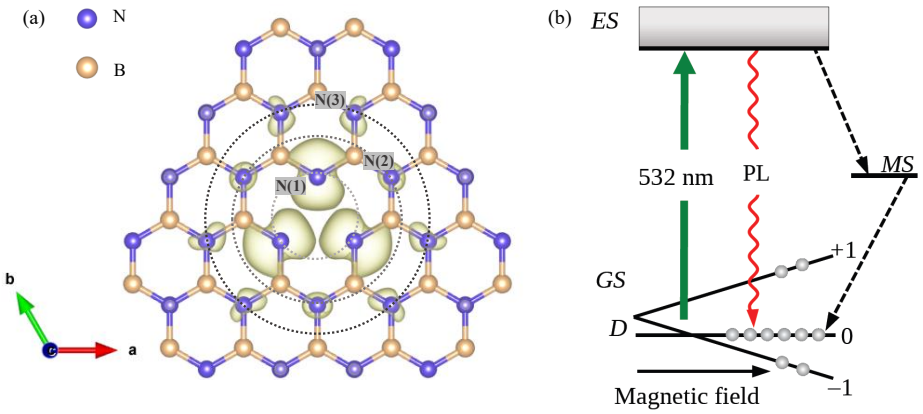

Figure 1. (a) hBN structure with a V_B^- defect (shown in red). The dotted lines show three spheres of nitrogen atoms (N(1), N(2), N(3)) closest to V_B^-. N(1) and N(2) contain three nitrogen atoms each, and N(3) contains 6 atoms. (b) Energy scheme of the levels of the optical pumping cycle of the spin sublevel $m_s = 0$ of the ground state (GS) of the V_B^- defect. The spin sublevels of the triplet are split in the zero magnetic field by the value D, shown by the curly bracket. Optical excitation at 532 nm (solid arrows) causes the transition of electrons from the ground state to the excited state (ES), after which they return to the ground state through optical recombination (PL, red wavy line) without changing the spin projection. Due to the presence of a metastable state (MS) in the system of levels, spin-dependent recombination occurs, indicated by dashed arrows, leading to a predominant population of $m_s = 0$ and allowing the electron spin of the boron vacancy to be read using the ODMR method by changing the intensity of the PL signal at the time of electron spin resonance (ESR).

spin states of point defects in hBN, which led to the identification of a wide range of defects with the property of optically induced preferential filling of spin sublevels [13–15]. This made it possible to implement highly coherent qubits based on them [16–18], approach the creation of electron-nuclear spin registers [15] by detecting and coherently controlling a single nuclear spin associated with a defect [15], and develop a number of highly sensitive subnanometer-scale quantum sensors due to the ability of hBN to be isolated at a monoatomic two-dimensional (2D) level [9,10,18]. It should be noted that the reproducibility of the formation of defects of a given type in hBN is of fundamental importance for the systematic study of their properties, the development of prototypes of devices based on them, as well as ensuring the stability of their characteristics and the results obtained. To date, it is precisely for the negatively charged boron vacancy in hBN that the possibility of reproducible defect formation with specified properties has been demonstrated, which is achieved by irradiating the material with high-energy particles (neutrons, electrons, protons, and light ions) [6,19–22]. An important feature of hBN is that its lattice consists of 100% magnetic nuclei (^{14}N, $I = 1$, n.a. 99.9%; ^{10}B, $I = 3$, n.a. 19.9%; ^{11}B, $I = 3/2$, n.a. 80.1%) with nuclear spin higher than $I = 1/2$. Consequently, they inevitably contribute to the spin Hamiltonian of the boron vacancy not only through hyperfine interactions (HFI), but also through nuclear quadrupole interactions (NQI) [6,23–25].

This circumstance leads, on the one hand, to significant losses in the coherence of the electron spin of the boron vacancy due to the above interactions, on the other hand, to interesting multiparticle quantum effects, pronounced in the behavior of the coherence of the vacancy spin

in small and high magnetic fields with a magnetic field boundary in the region of 1 T, as it was theoretically and experimentally shown in works [26,27]. An important feature of electron-nuclear interactions in such systems is that using standard electron spin resonance methods it is impossible to directly obtain information about nuclear quadrupole interactions due to the fact that the latter do not contribute to the electron spin resonance signal according to the selection rules for allowed magnetic dipole transitions ($\Delta m_S = \pm 1$; $\Delta m_I = 0$). Thus, studies of electron-nuclear interactions in such high-spin systems require methods related to the observation of nuclear magnetic resonance (NMR) signals with selection rules ($\Delta m_S = 0$; $\Delta m_I = \pm 1$). Such a method is electron-nuclear double resonance (ENDOR), which makes it possible to register nuclear spin flips by changing the intensity of the electron spin resonance signals in accordance with the selection rules ($\Delta m_S = 0$; $\Delta m_I = \pm 1$), which is achieved by applying an additional saturating radio frequency field resonant with transitions between the nuclear spin sublevels of atoms associated with the electron spin of the defect through hyperfine and nuclear quadrupole interactions. Schematically, the structure of energy levels and NMR transitions in the system ($S = 1$; $I = 1$) is shown in Fig. 2, according to the spin Hamiltonian (1) describing the V_B^- center:

$$\hat{H} = g\mu_B B_0 S_z + D\left(S_z^2 - \frac{S(S+1)}{3}\right) + \\ + \sum_{j=1}^{3}\left(A_{zz}S_z I_{z(i)} + A_{xx}S_x I_{x(i)} + A_{yy}S_y I_{y(i)} - \gamma\hbar B_0 I_z + \frac{\chi_{iq}}{4I(2I-1)}\left(3I_{z(i)}^2 - I(I+1)\right)\right), \quad (1)$$

where the first two terms describe the Zeeman and fine interactions, A_{xx}, A_{yy}, A_{zz} are the energies of the hyperfine interaction of the V_B^- defect electron and surrounding nuclei, respectively reflecting the isotropic ($A_{iso} = \frac{1}{3}(A_{xx} + A_{yy} + A_{zz})$) and the anisotropic part of HFI ($A_{dd} = \frac{1}{6}(2A_{zz} - A_{xx} - A_{yy})$), γ is the gyromagnetic ratio for the nuclear magnetic moment ($\gamma(^{14}\mathrm{N}) = 1.93 \cdot 10^7\,\mathrm{rad{\cdot}s^{-1}{\cdot}T^{-1}}$), $\chi_{iq} = \frac{e}{h} \cdot Q_N \cdot V_{zz}$ is the nuclear quadrupole splitting constant characterizing the interaction of the nuclear electric quadrupole moment ($e \cdot Q_N$) with the electric field gradient (EFG) at the nuclear point (V_{zz}, the main component of the EFG tensor), $\eta = \frac{V_{xx} - V_{yy}}{V_{zz}}$ is the anisotropy of this interaction. Summation by i includes all the surrounding nuclei. It is worth noting that the level scheme shown in Fig. 2 is expected in the case when all nuclear magnetic moments are equivalent, which should be expected when the vector of an external magnetic field induction is directed parallel to the hexagonal axis of the crystal ($B_0 \parallel c$). In this paper, we present the results of a study of the interaction of the electric field gradient caused by the presence of a boron vacancy in hBN with quadrupole nuclear magnetic moments of nitrogen atoms located outside the first coordination sphere of nitrogen atoms, indicated in Fig. 1(a) as N(1). To determine the symmetry of the NQI and the parameters of the corresponding tensor, we studied NMR transitions (shown in maroon in Fig. 2(a)) between nuclear spin sublevels to a state with the projection of the electron spin of the boron vacancy $m_S = 0$ by the ENDOR method.

This approach makes it possible to directly register exclusively the contribution from the nuclear quadrupole interaction due to the fact that there is no HFI for the state with a zero projection of the electron spin, as can be seen from the spin Hamiltonian (1). At the same time, in the ENDOR spectra, according to the level scheme in Fig. 2, there should be two pairs of lines from each electronic transition. One pair of lines centered around the Larmor precession frequency of the nuclear magnetic moment ^{14}N, $\nu_L = \frac{\gamma}{2\pi}B_0 \approx 10\,\mathrm{MHz}$ (in the W-band at $B_0 \approx 3.3\,\mathrm{T}$) with a distance between them equal to the magnitude of the quadrupole

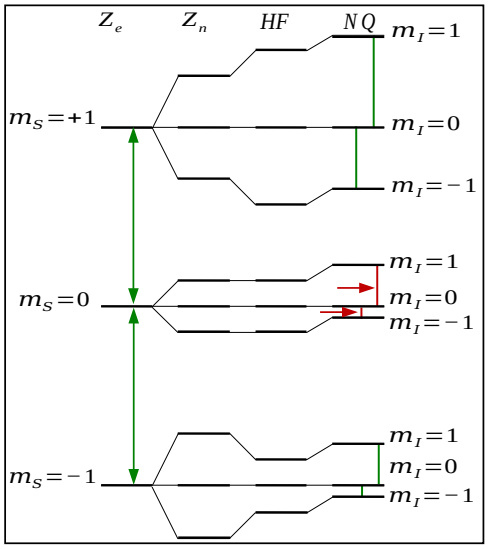

Figure 2. Energy levels of the V_B^- defect interacting with ^{14}N nuclear spins, including electron Zeeman fission (Z_e) and zero-field fission, hyperfine interaction (HF), nuclear quadrupole interaction (NQ) and nuclear Zeeman interaction (Z_n). The levels are marked with the corresponding quantum numbers m_S; m_I. The allowed ESR transitions are shown by vertical arrows. NMR transitions are shown by green (for $m_S = \pm 1$) and maroon (for $m_S = 0$) lines. The maroon horizontal arrows indicate NMR transitions caused solely by the quadrupole interaction with ^{14}N. (b) The ESR spectra of V_B^- defects recorded in the electron spin echo mode with $B \parallel c$ magnetic field orientation and optical laser pumping of $\lambda = 532$ nm. The transitions of the fine structure between the spin sublevels of the triplet with splitting in a magnetic field equal to ΔB, equal to twice the splitting value in a zero magnetic field, D, are shown by the horizontal arrow. The inset schematically shows the optically induced population of the sublevel $m_S = 0$, which causes phase inversion of the spin echo signals of boron vacancies.

splitting, and the second with an offset by the value of HFI and the the same distance between the lines. Due to the different m_S sign, the offset will be in different directions for different electronic transitions.

2. The research methods

Commercial hBN (HQ Graphene) single crystals irradiated with 2 MeV electrons at a dose of $6 \cdot 10^{18}$ cm^{-2} were used to generate V_B^- defects [19]. Experimental studies were performed on a Bruker Elexsys 680 W-band (94 GHz) EPR spectrometer at a temperature of $T = 25$ K. The electronic paramagnetic resonance (EPR) detected by the electron spin echo (ESE) was recorded using the standard Hahn pulse sequence $\frac{1}{2}\pi$(MW)–τ–π(MW)–τ–ESE with a duration of $\frac{\pi}{2}$(MW) pulse of 48 ns and a value of $\tau = 300$ ns. The standard Mims ENDOR pulse sequence

$$\frac{1}{2}\pi(\mathrm{MW}) - \tau - \frac{1}{2}\pi(\mathrm{MW}) - t_1 - \pi(RF) - t_2 - \frac{1}{2}\pi(\mathrm{MW}) - \tau - \mathrm{ESE}$$

was used for probing nuclear spins [28]. The first two $\frac{\pi}{2}$(MW) microwave pulses induced population inversion of the electron spin levels; the third $\frac{\pi}{2}$(MW) pulse provided the formation of a stimulated spin echo (SSE) signal. In the interval between the second and third microwave pulses 50 μs, a radio frequency pulse π_{RF} ($t_{RF} = 44\,\mu$s) was applied, which caused the inversion of populations of nuclear spin sublevels and induced NMR transitions. NMR frequencies were calculated using EasySpin software [29].

The simulations were performed using a periodic hexagonal boron nitride (hBN) supercell containing 511 atoms ($8\times8\times2$ unit cells with 4 BN layers) with one embedded V_B^- defect. Within

the density functional theory (DFT) framework, the quadrupole coupling constant was computed by evaluating the electric field gradient (EFG) at the defect site using the Gauge-Including Projector Augmented-Wave (GIPAW) method, as implemented in the Quantum ESPRESSO software package. The calculations employed the Perdew-Burke-Ernzerhof (PBE) exchange-correlation functional, ultrasoft pseudopotentials for boron, nitrogen, and vacancy sites, and a plane-wave basis set with a kinetic energy cutoff of 600 eV.

3. Results and Discussion

As a result of irradiation, boron vacancies in the negative charge state were created in hBN crystals, as evidenced by the ESR spectrum recorded with the orientation of an external magnetic field directed parallel to the hexagonal axis c ($B_0 \parallel c$), shown in Fig. 3(a). Indeed, the signals indicated by the arrow on the spectrum are characterized by splitting along the magnetic field ΔB, which corresponds to twice the amount of splitting of the spin sublevels of the triplet ($S = 1$) in the zero magnetic field, schematically indicated in the inset of Fig. 3(a) as D. Namely, $\Delta B = \dfrac{2D}{g\mu_B} = 255\,\text{mT}$, where $D = 3.57\,\text{GHz}$ the value of zero field spliting (ZFS), g is the electronic g-factor $g = 2.00$, and μ_B is the Bohr magneton. The parameters D and g correspond to the previously determined methods of microwave spectroscopy [6, 19]. The first step for the research was the study of NQI with nitrogen nuclei removed from the boron vacancy. We recorded the ENDOR spectra on both components of the fine structure corresponding to the transitions $m_S : 0 \leftrightarrow +1$ and $m_S : 0 \leftrightarrow -1$ and indicated in Fig. 3(a). As expected, according to the level scheme shown in Fig. 2, the ENDOR spectra contain eight NMR transitions shown in Fig. 3(b,c,d,e). We also note that different electronic transitions are observed at significantly different values of magnetic field inductions B_0, and the position of ν_L differs significantly. The values HF and NQ can be determined at from the position of the NMR frequencies of 4.41 MHz and 0.37 MHz, respectively.

To determine the symmetry and absolute magnitudes of the NQI tensor of the V_B^- center with removed ^{14}N atoms, the angular dependence of NMR transitions in the electron spin state $m_S = 0$ in the ENDOR spectra was studied when the magnetic field induction vector rotates from $B_0 \parallel c$ to orientation $B_0 \perp c$, corresponding to the case when the field vector lies in the (0001) plane of a two-dimensional hBN sheet.

With this rotation, the magnetic nuclei become non-equivalent, and each ^{14}N nucleus produces two lines in the ENDOR spectra. Thus, in the case of studying interactions with nuclear spins in the nitrogen sphere, designated as N(2) in Fig. 1, it is expected to see 6 lines in the NMR spectrum for each sublevel of m_S, whereas in the case of interaction with nuclear spins in the sphere of N(3), it is expected to observe a set of 12 NMR lines in the ENDOR spectra. The results of such measurements, together with the calculated course of the angular dependence of the lines, are shown in Fig. 4(a) shows the spectra recorded with the orientation of the magnetic field $B_0 \parallel c$. The NMR signals correspond to the transitions $m_I : 0 \leftrightarrow +1$ and $m_I : 0 \leftrightarrow -1$ induced by radio frequency in the state with $m_S = 0$ and correspond to the signals shown in Fig. 3(d,c). The dependence of the position of the lines in the ENDOR spectra on the magnetic direction, calculated in the EasySpin program, is shown in Fig. 4(b). The angular dependence shows that each pair of lines registered in the $B_0 \parallel c$ orientation, corresponding to the case when all magnetic moments are equivalent, splits into 12 lines as the angle increases. The course of the lines in angular dependence and the spectra recorded in the orientation $B_0 \perp c$ shown in Fig. 4(c) is described by the quadrupole interaction parameter $\chi_q = 0.37\,\text{MHz}$ and $\eta = 0.55$. Values

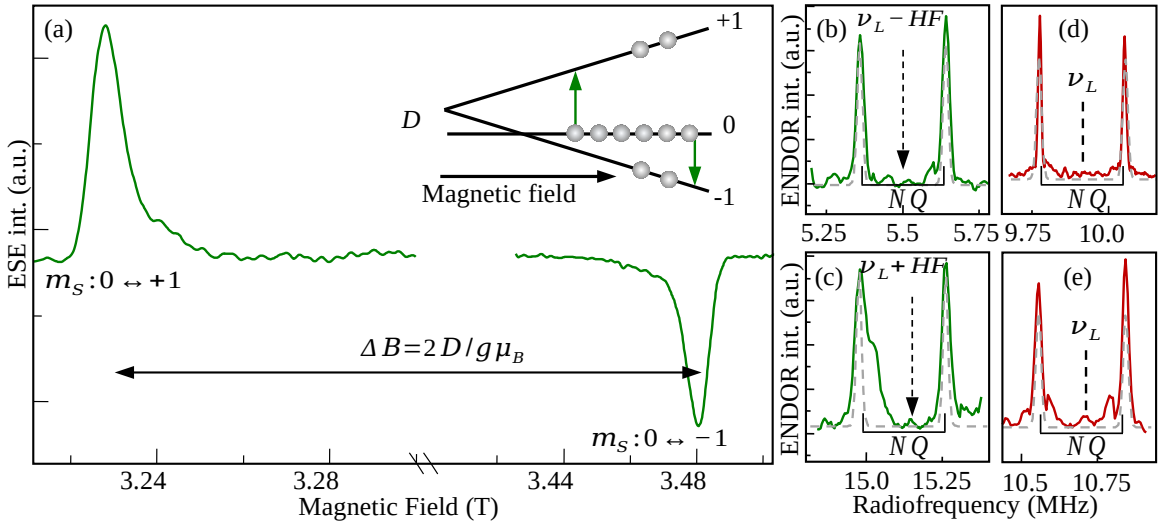

Figure 3. (a) The ESR spectrum of V_B^- defects recorded in the electron spin echo mode with $B_0 \parallel c$ magnetic field orientation and optical laser pumping of $\lambda = 532$ nm. The transitions of the fine structure between the spin sublevels of a triplet with splitting in a magnetic field equal to ΔB, (twice the amount of splitting in a zero magnetic field, $2D$) are shown by a horizontal arrow. The inset schematically shows the optically induced population of the sublevel $m_S = 0$, which causes phase inversion of the spin echo signals of boron vacancies. (b,c,d,e) ENDOR spectra recorded on the components of the fine structure of V_B^- defects. The experimental data are shown in green and maroon, and the calculated spectra using the spin Hamiltonian (1) are shown as a gray dotted line. The NMR signal frequencies in Figures (b) and (c) correspond to NMR transitions between hyperfine sublevels at the electron spin sublevels $m_S = +1$ (b) and $m_S = -1$ (c), according to the selection rules $\Delta m_S = \pm 1$ for allowed transitions and the frequencies at (d) and (e) between the quadrupole-split nuclear sublevels to the state with the projection of the electron spin $m_S = 0$. The position of the Larmor precession frequency ^{14}N, ν_L, is indicated by a dotted arrow. The split between the pairs of lines on each panel is caused by NQI and is designated as NQ. The shift of the quadrupole split lines by the value of HFI (HF) is indicated on panels (b) and (c) by the dotted arrows $\nu_L \pm HF$

calculated by the density functional theory method $\chi_q = 0.47$ MHz and $\eta = 0.58$. It is worth noting that these experimental data on the measurement of the V_B^- center NQI using exclusively split nuclear spin sublevels are in good agreement with previously obtained measurements of the ENDOR spectra on states with an admixture of hyperfine interaction corresponding to the projections of the electron spin $m_S = \pm 1$ [30]. The latter provides an additional resource for comparing and verifying the values of the directly measured value of the NQI with nitrogen atoms, which can be done by analyzing the ENDOR spectra measured using a nonzero projection of the electron spin of the boron vacancy. So, Fig. 5 shows the ENDOR spectra measured for the state $m_S = -1$ at the orientation of the magnetic field $B_0 \perp c$. Its theoretical description using the spin Hamiltonian (1) with the parameters of the nuclear quadrupole interaction obtained from the ENDOR description shown in Fig. 4 and the hyperfine interaction constants is clearly indicative of the accuracy of determining the value of the NQI. Additionally, it is worth noting the pronounced structure of the spectrum in Fig. 5, containing 12 lines. This corresponds to 6 unequal nitrogen atoms in the orientation $B_0 \perp c$ and clearly indicates that the gradient of the crystal field was studied on the atoms of the third sphere, indicated in Fig. 1 as N(3).

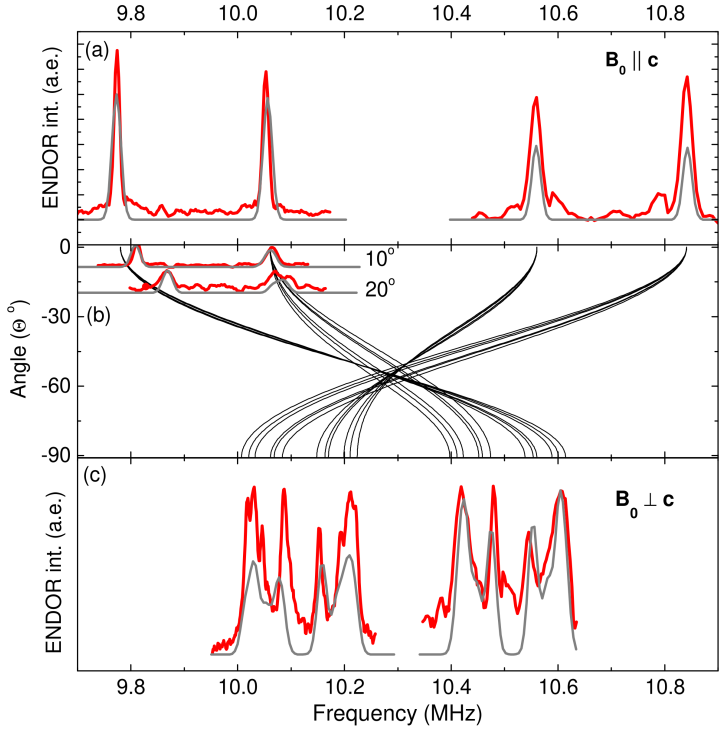

Figure 4. (a) ENDOR spectra recorded on both components of the fine structure of V_B^- defects in the orientation of the magnetic field $B_0 \parallel c$ at the sublevel $m_S = 0$. The spectra correspond to those shown in Fig. 3 (d,e) at $B_0 = 3221.4$ and 3476.5 mT. (b) Calculation of the angular dependence of the line paths in the ENDOR spectra upon rotation of the magnetic field induction vector from parallel to perpendicular orientation relative to the c axis of the crystal. (c) ENDOR spectra measured at orientation $B_0 \perp c$ at $B_0 = 3289.8$ and 3415.5 mT. The calculation of the spectra at $B_0 \parallel c$ and $B_0 \perp c$ is shown by gray lines.

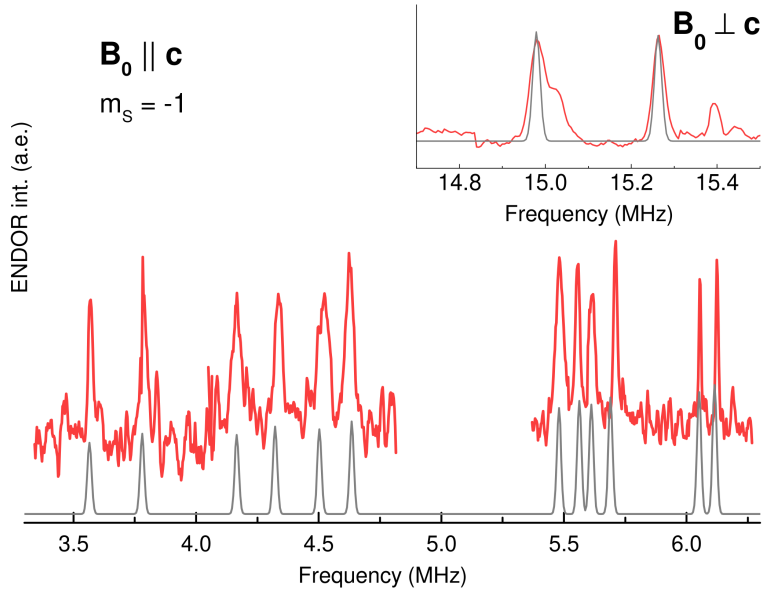

Figure 5. The ENDOR spectra recorded at the orientation of the magnetic $B_0 \perp c$ ($B_0 = 3289.8$ mT) at the sublevel with the projection of the electron spin $m_S = -1$. The set of 12 NMR transitions is numbered accordingly. The calculated ENDOR spectra obtained using the Hamiltonian (1) and the parameters $\chi_q = 0.37$ MHz; $\eta = 0.55$ MHz; $A_{iso} = 5.23 \pm 0.03$ MHz, $A_{dd} = 0.82 \pm 0.03$ MHz is shown in gray lines.

4. Summary

In the present work, we have investigated NQI with removed nitrogen atoms located in the third coordination sphere of the V_B^- defect. A certain value of the NQI constant is set to $\chi_q = 0.37$ MHz, which is significantly less than the interaction with ^{14}N located in the first coordination sphere of the boron vacancy (N(1) in Fig. 1(a)), previously set to $\chi_q \approx 1.5$ MHz [24]. This observation reflects the fact that as we move away from the vacancy, the electron density associated with the defect becomes small and makes a minimal contribution to the distortion of the hBN's own electric field. Thus, the spin density of the boron vacancy opens up the possibility of probing the internal nuclear properties of hBN using microwave spectroscopy methods. For example, a single NV defect in diamond was previously used as a spin probe to study the constants of the nuclear quadrupole interaction in hBN. The dynamics of its spin coherence, recorded using the XY8 pulse sequence, made it possible to study the parameters of quadrupole interactions in hBN, in particular, it was possible to experimentally establish the quadrupole interaction constant for the intrinsic nuclei of the isotope ^{11}B of the lattice ($\chi_q(^{11}\mathrm{B}) = 2.9221 \pm 0.0006$ MHz). In this context, the V_B^- defect can play the role of its own spin probe in the hBN lattice, which will allow alternative and complementary studies of its spin fundamental properties.

Acknowledgments

Financial support of the Russian Science Foundation under Grant RSF 24-72-00161 is acknowledged.

References

1. Cassabois G., Valvin P., Gil B., *Nature Photonics* **10**, 262 (2016).

2. Caldwell J. D., Aharonovich I., Cassabois G., Edgar J. H., Gil B., Basov D. N., *Nature Reviews Materials* **4**, 552 (2019).

3. Ren W., Boggild P., Redwing J., Novoselov K., Sun L., Qi Y., Jia K., Liu Z., Burton O., Alexander-Webber J., Hofmann S., Cao Y., Long Y., Yang Q.-H., Li D., Choi S. H., Kim K. K., Lee Y. H., Li M., Huang Q., Gogotsi Y., Clark N., Carl A., Gorbachev R., Olsen T., Rosen J., Sommer Thygesen K., Efetov D. K., Jessen B. S., Yankowitz M., Barrier J., Krishna Kumar R., Koppens F. H. L., Deng H., Li X., Dai S., Basov D. N., Wang X., Das S., Duan X., Yu Z., Borsch M., Ferrari A. C., Huber R., Kira M., Xia F., Wang X., Wu Z.-S., Feng X., Simon P., Cheng H.-M., Liu B., Xie Y., Jin W., Raveendran Nair R., Xu Y., Zhang Q., Katiyar A. K., Ahn J.-H., Aharonovich I., Hersam M. C., Roche S., Hua Q., Shen G., Ren T., Zhang H.-B., Koo C. M., Koratkar N., Pellegrini V., Young R. J., Qu B., Lemme M., Pollard A. J., *arXiv preprint arXiv:2503.22476* (2025).

4. Wang Q. H., Bedoya-Pinto A., Blei M., Dismukes A. H., Hamo A., Jenkins S., Koperski M., Liu Y., Sun Q.-C., Telford E. J., Kim H. H., Augustin M., Vool U., Yin J.-X., Li L. H., Falin A., Dean C. R., Casanova F., Evans R. F. L., Chshiev M., Mishchenko A., Petrovic C., He R., Zhao L., Tsen A. W., Gerardot B. D., Brotons-Gisbert M., Guguchia Z., Roy X., Tongay S., Wang Z., Hasan M. Z., Wrachtrup J., Yacoby A., Fert A., Parkin S., Novoselov K. S., Dai P., Balicas L., Santos E. J. G., *ACS Nano* **16**, 6960 (2022).

5. Boretti A., Blackledge J., Castelletto S., *Materials Science in Semiconductor Processing* **185**, 108932 (2025).

6. Gottscholl A., Kianinia M., Soltamov V., Orlinskii S., Mamin G., Bradac C., Kasper C., Krambrock K., Sperlich A., Toth M., Aharonovich I., Dyakonov V., *Nature Materials* **19**, 540 (2020).

7. Novoselov K. S., Mishchenko A., Carvalho A., Castro Neto A., *Science* **353**, aac9439 (2016).

8. Chejanovsky N., Mukherjee A., Geng J., Chen Y.-C., Kim Y., Denisenko A., Finkler A., Taniguchi T., Watanabe K., Dasari D. B. R., Auburger P., Gali A., Smet J. H., Wrachtrup J., *Nature Materials* **20**, 1079 (2021).

9. Gottscholl A., Diez M., Soltamov V., Kasper C., Krause D., Sperlich A., Kianinia M., Bradac C., Aharonovich I., Dyakonov V., *Nature Communications* **12**, 4480 (2021).

10. Vaidya S., Gao X., Dikshit S., Aharonovich I., Li T., *Advances in Physics: X* **8**, 2206049 (2023).

11. Tabesh F., Fani M., Pedernales J., Plenio M., Abdi M., *Physical Review B* **107**, 214307 (2023).

12. Gao X., Vaidya S., Li K., Ge Z., Dikshit S., Zhang S., Ju P., Shen K., Jin Y., Ping Y., Li T., *Nature Materials* **21**, 1024 (2022).

13. Mendelson N., Chugh D., Reimers J. R., Cheng T. S., Gottscholl A., Long H., Mellor C. J., Zettl A., Dyakonov V., Beton P. H., Novikov S. V., Jagadish C., Tan H. H., Ford M. J., Toth M., Bradac C., Aharonovich I., *Nature Materials* **20**, 321 (2021).

14. Stern H. L., Gilardoni C. M., Gu Q., Barker S. E., Powell O. F. J., Deng X., Fraser S. A., Follet L., Li C., Ramsay A. J., Tan H. H., Aharonovich I., Atature M., *Nature Materials* **23**, 1379 (2024).

15. Gao X., Vaidya S., Li K., Ge Z., Dikshit S., Zhang S., Ju P., Shen K., Jin Y., Ping Y., Li T., *Nature* , 1 (2025).

16. Rizzato R., Schalk M., Mohr S., Hermann J. C., Leibold J. P., Bruckmaier F., Salvitti G., Qian C., Ji P., Astakhov G. V., Kentsch U., Helm M., Stier A. V., Finley J. J., Bucher D. B., *Nature Communications* **14**, 5089 (2023).

17. Haykal A., Tanos R., Minotto N., Durand A., Fabre F., Li J., Edgar J. H., Ivády V., Gali A., Michel T., Dréau A., Gil B., Cassabois G., Jacques V., *Nature Communications* **13**, 4347 (2022).

18. Vogl T., Ivdy V., Luxmoore I. J., Stern H. L., *arXiv preprint arXiv:2510.04344* (2025).

19. Murzakhanov F. F., Yavkin B. V., Mamin G. V., Orlinskii S. B., Mumdzhi I. E., Gracheva I. N., Gabbasov B. F., Smirnov A. N., Davydov V. Y., Soltamov V. A., *Nanomaterials* **11**, 1373 (2021).

20. Murzakhanov F. F., Mumdzhi I., Mamin G. V., Yusupov R. V., Davydov V. Y., Smirnov A. N., Muzafarova M. V., Nagalyuk S. S., Soltamov V. A., *Physics of the Solid State* **64**, 210 (2022).

21. Hennessey M., Whitefield B., Gale A., Kianinia M., Scott J. A., Aharonovich I., Toth M., *Advanced Quantum Technologies* **8**, 2300459 (2025).

22. Latypova L., Murzakhanov F., Mamin G., Sadovnikova M., von Bardeleben H. J., Gafurov M., *Quantum Reports* **6**, 263 (2024).

23. Mamin G., Dmitrieva E., Murzakhanov F., Gracheva I., Soltamov V., Gafurov M., *Magnetic Resonance in Solids* **27**, art. 25102 (2025).

24. Murzakhanov F. F., Mamin G. V., Orlinskii S. B., Gerstmann U., Schmidt W. G., Biktagirov T., Aharonovich I., Gottscholl A., Sperlich A., Dyakonov V., Soltamov V. A., *Nano Letters* **22**, 2718 (2022).

25. Gracheva I. N., Murzakhanov F. F., Mamin G. V., Sadovnikova M. A., Gabbasov B. F., Mokhov E. N., Gafurov M. R., *The Journal of Physical Chemistry C* **127**, 3634 (2023).

26. Tarkanyi A., Ivady V., *arXiv preprint arXiv:2505.03292* (2025).

27. Lee J., Kim H., Park H., Seo H., *Advanced Functional Materials* , e11274 (2025).

28. Mims W., *Physical Review B* **5**, 2409 (1972).

29. Stoll S., Schweiger A., *Journal of Magnetic Resonance* **178**, 42 (2006).

30. Mamin G., Dmitrieva E., Murzakhanov F., Gracheva I., Mokhov E., Vlasov I., Gafurov M., Gerstmann U., Soltamov V., *Applied Physics Letters* **127**, art. 024001 (6 pp) (2025).